Effect of pH on Hydrothermal Synthesis of ZrO₂ Nanoparticles and their Electrocatalytic Activity for Hydrogen Production

Q. Mohsen[1,], Wael S. Al-Gethami[1], Z. Zaki[1], S.H. Alotaibi[1], Mohamed M. Ibrahim[1], Mohamed Ezzat[1], Mohammed A. Amin[1], M. M. Kamel[3], Nasser Y. Mostafa[3,*]*

[1] Materials and Corrosion Group, Department of Chemistry, Faculty of Science, Taif University, Saudi Arabia
[2] Department of Chemistry, Faculty of Turabah University College, Taif University, Turabah 21995, Saudi Arabia
[3] Department of Chemistry, Faculty of Science, Suez Canal University, Ismailia 41522, Egypt
[*]E-mail: [1]mohsen@tu.edu.sa & [3]nmost69@yahoo.com

Electrolytic hydrogen production needs heavy-duty electrocatalyst to lower the overpotential to economical values. With this respect, we scrutinized the effect of pH on the phase formation, microstructure and hydrogen production activity of ZrO_2 generated under hydrothermal processing. At both low and high pHs (2.61 and 14) the products are single phase monoclinic ZrO_2. However, at intermediate pHs (7.0-11.0), the produces are biphasic mixture of tetragonal and monoclinic nano crystallites. The particles size slightly increases (from 11 to 14 nm) with increasing the pH up to 11. However, at pH=14.0, the particle size abruptly increases to 98 nm. The vibration spectra demonstrated that monoclinic ZrO_2 comprise intense surface hydroxyl functional groups, that enhance the electrocatalytic activity of ZrO_2 nanoparticles. Thus, the hydrogen evolution activity increases with increasing the monoclinic phase contents. ZrO_2 produced at low pH (2.61) showed the highest electrocatalytic activity.

1. INTRODUCTION

Nowadays, it is clearly evident that there is an anthropogenic climate change due to the warming of the earth's surface. Undoubtedly, these effects are attributed mainly to the extensive burning of fossil fuels and the release of carbon dioxide (CO_2) [1]. In this regard, researchers have been extensively investigating all possible alternatives clean energy resources [2] and all possible ways to storage the renewable energy. Hydrogen constitutes one of the best solutions which can be adopted in the future to overcome the current environmental contamination as it is associated with a high gravimetric energy

density which helps store energy. Over decades, hydrogen evolution reaction (HER) have intensively investigated due to being the core of water splitting process [3]. Currently, the process of producing hydrogen relies on the highly active and selective development of catalysts [4].

Zirconium oxide (ZrO_2) has many technological applications due to its mechanical and chemical features. For example, its surface stability in both basic and acidic media and stability at high temperatures. In addition, zirconia has a high resistivity against oxidation and low thermal conductivity. Moreover, it is mechanically strong [5, 6] and it is porosity is controllable. In fact, zirconia is an effective oxide material because of having a high degree of electrical resistance; therefore, it can be utilized as a ceramic insulator [7, 8]. Different forms of zirconia are used as catalyst for many major reactions such as oxidation, elimination, hydrogenation, and dehydration. The acidic active sites in zirconia catalyst [9, 10] are essential for acceleration several reactions such as hydrocracking, alkene, alkylation, and isomerization [11, 12]. In addition, different doped zirconia have high thermal stability with high ionic conductivity [13]. Both features have led to the utilization of zirconia in oxygen sensors and refractories [14, 15]. Because of its biocompatibility, zirconia is used as a key element of orthopedic implants [16-18]. Generally, ZrO_2 crystallizes in three forms; cubic, tetragonal and monoclinic [19]. The stability of the cubic phase occurs at temperatures exceed 2370°C up to melting point. In this phase, the structure, which is accompanied by a 5.27Å unit cell, is fluorite. It is noticeable that a group of eight oxygen atoms is associated with each Zr^{+4} ion, and four atoms of zirconium are associated with each of these eight oxygen atoms. The bond between the oxygen atoms and zirconium atoms is in the form of a tetrahedral manner [20, 21].

The technology advances always need now materials with tailor-made properties [22]. Solution based chemical synthesis provide numerous advantages in tailoring materials properties by controlling the synthesis parameter, such as temperature, pH and surfactants addition [23]. Solvothermal method firstly discovered in geological formation of minerals [24]. Now days, it is commonly used in production of many technological materials, such as quartz single crystals [25, 26] calcium silicate hydrates [23] and zeolites [27]. The method depends on the directly precipitation of pure crystalline materials from solvent under high temperatures and pressures without calcination step [28, 29].

In the current article, the synthesis of highly active hydrogen evolution reaction (HER) electrocatalyst based on hydrothermally prepared ZrO_2 nanoparticles was investigated. The influence of pH variation on the phase formed and microstructure of ZrO_2 was investigated, as well as the catalytic activity of hydrogen production.

2. EXPERIMENTAL

2.1 Chemicals

The used chemicals were analytical grade. Sodium hydroxide (NaOH) and Zirconyloxychloride octahydrate ($ZrOCl_2.8H_2O$) was obtained from Sigma- Aldrich.

2.2 Synthesis of zirconium oxide nanoparticles:

Hydrothermal method was used to obtain nanoparticles of ZrO_2. 2.22 gams of $ZrOCl_2.8H_2O$ was dissolved in 400 mL of distilled water. The measured pH was 2.61. The solution was hydrothermally cured in 600 mL Teflon coated home-made stainless steel autoclaved for 24 hours. The external temperature of the autoclave is mentioned 240°C using external heat controller. The previous steps were repeated with adjusting the pH to 7, 11, and 14 by sodium hydroxide solution (NaOH). After opening the autoclave, we obtained a soft white precipitate which washed several times and separated using a centrifuge.

2.3 Characterization:

X-ray diffraction (XRD) were examined using Bruker diffractometer (D8-advance) with Cu-K$_\alpha$ radiation. FWHM was calculated by X'Pert HighScore Plus program. Lattice constants were determination by Least squares refinement of the X-ray diffraction data using X'Pert HighScore Plus. The high-resolution transmission electron microscopy (HR-TEM) is conducted by passing this beam through the specimen and collecting the image to be displayed on a screen (220 KV). The scanning electron microscopy (SEM) is conducted by detecting the electrons and transmitting the electrical signal to a video screen. ATR- FTIR measurements were done with Alpha-P Spectrometer (Bruker, Germany).

2.4 Electrocatalytic activity measurements:

The catalysts suspensions were prepared by sonicating 4.0 mg of ZrO_2 catalysts with 0.5 ml ethanol for 10 min. Then 0.50 ml of Nafion solution (0.25%) was included with further sonication for 10 min. The catalysts suspensions were loaded on glassy carbon electrodes with *3*.00 mm diameter and dried. The load densities were 2.8 μg/cm^2 for all catalysts.

Linear sweep voltammetry (LSV) techniques were employed to estimate the electrochemical hydrogen production activity of different phases of ZrO_2 catalysts. The three-electrode system was used in all electrochemical investigations. The reference electrode was a saturated calomel electrode (SCE) and the auxiliary electrode was a graphite rod. Air-free aqueous 1.0 M NaOH solutions and Autolab (PGSTAT30/FRA) potentiostat was used in all measurements. A temperature-controlled bath was used to adjust the temperature at room temperature (≈25 °C).

3. RESULTS AND DISCUSSION

3.1 XRD analysis

The effect of pH, on the formation of different phases of the ZrO_2 prepared by hydrothermal technique, was investigated by the XRD analysis. Fig 1 shows that the products are different phases of ZrO_2 (monoclinic and tetragonal structure). All the diffraction peaks are in good agreement either with JCPDS card of monoclinic (JCPDS Card no. 01-083-0940 space group P21/c) or tetragonal ZrO_2 (JCPDS

Card no. 01-079-1769 space group P42/c). The diffraction peaks at 2θ values of 24.13 ,28.29, 30.20,30.39, 31.39, 34.26,35.21, 41.16, 45.08, 50.08, 55.56, 60.0 and 63.0 correspond to monoclinic ZrO_2 phase and 24.13 ,28.29, 30.20, 31.39, 34.26, 41.16, 45.08, 50.08, 55.56 and 60.0 correspond to tetragonal ZrO_2 phase [30].
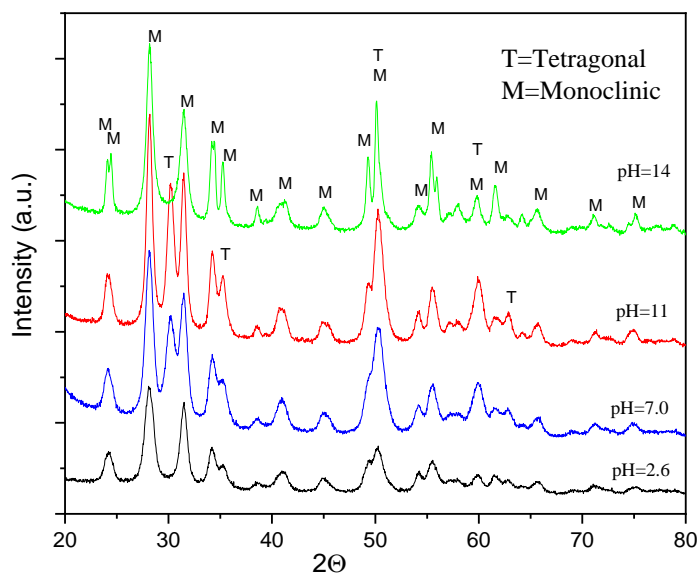
Figure 1. XRD patterns of ZrO_2 formed at various pHs..

In case of pH = 2.61 the peaks are for a pure monoclinic phase, as previously found [10]. However, for sample prepared at higher pH (7-11), both monoclinic and tetragonal ZrO_2 are formed. The percentage of tetragonal phase increase with increasing pH up to 11. At very high pH (14) only monoclinic ZrO_2 is formed [31]. The phase composition of the prepared $ZrO_2$are given in Table 1 as determined from XRD data analysis.

Table 1. Phase composition of ZrO2 hydrothermally prepared at different pH.

pH value	2.6	7.0	11.0	14.0
Monoclinic ZrO_2 (%)	100	83	71	100
Tetragonal ZrO_2 (%)	0.0	17	29	0.0

The main conclusion from XRD is that at low pH value (2.61) and high pH value (14) the products are single monoclinic phase. However, at intermediate pHs (7-11) the produces are mixture of both monoclinic and tetragonal crystals.

3.2. Microstructure:

High-resolution TEM micrographs have been shown in Figure 2-5. All ZrO_2 samples show the particles in nono size range. It is clear from the Figs that the particles size increases with increasing the pH. The particles size slightly increases (from 11 to 14 nm)) with increasing the pH[32][31][30][29][32][31][30][32][31][30][29][32][32][32][32][31][30][32][32] up to 11. However, at pH=14.0, the particle size abruptly increases to 98 nm. Fig. 2 shows the continuous parallel lattice fringes at different areas implying ZrO_2 crystals are perfectly formed by sluggish oriented and growth process under hydrothermal conditions. The distance between the parallel fringes is either 0.316 nm or 0.262 nm, which match well with (-111) and (111) Miller index, respectively of ZrO_2 with monoclinic lattice.

Fig. 3 and Fig. 4, shows zirconia catalysts produced at pH=7 and 11, respectively. The pictures show spherical morphology and average diameter 12.99 nm and 14.76 14.76 nm for pH=7 and 11, respectively (see Table 2). Fig. 5 illustrates HRTEM image of ZrO_2 prepared at pH=14. The main particle characteristic is the elongated morphology with aspect ratio of 2.61 (average length = 98.77 and average wide = 37.57 nm). The perfectly oriented lattice fringes with successive distances 0.316 nm, approves that the nanocrystals composed of monoclinic zirconia phase.
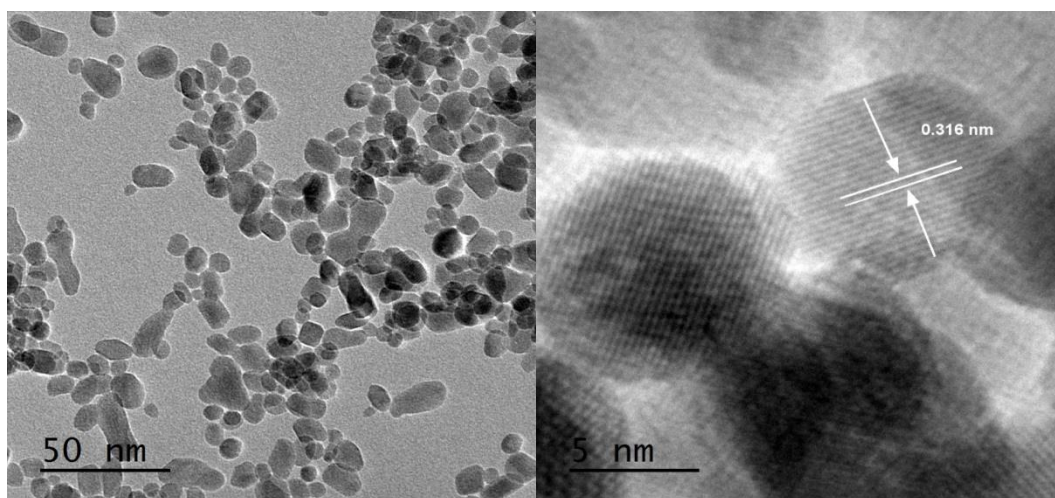
Table 2. The average of particles size of ZrO_2 prepared at different pH.

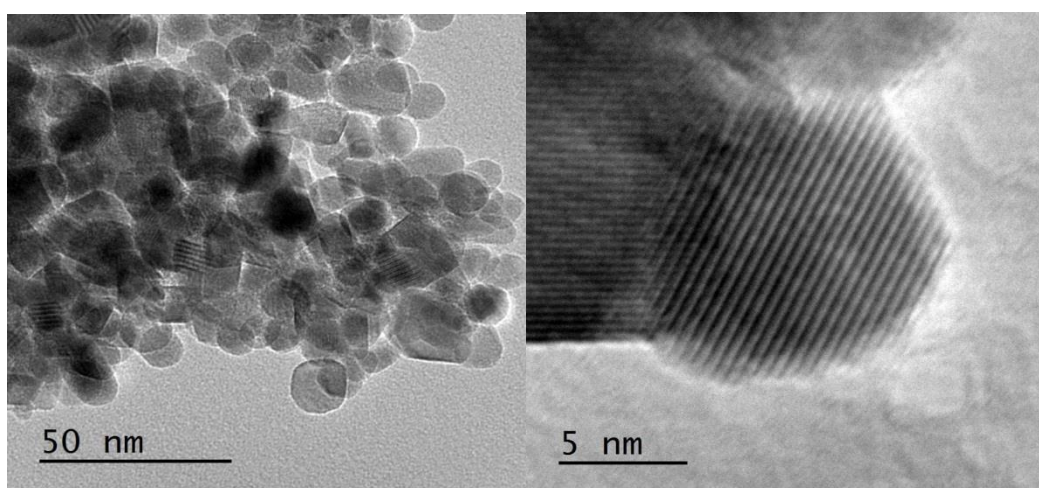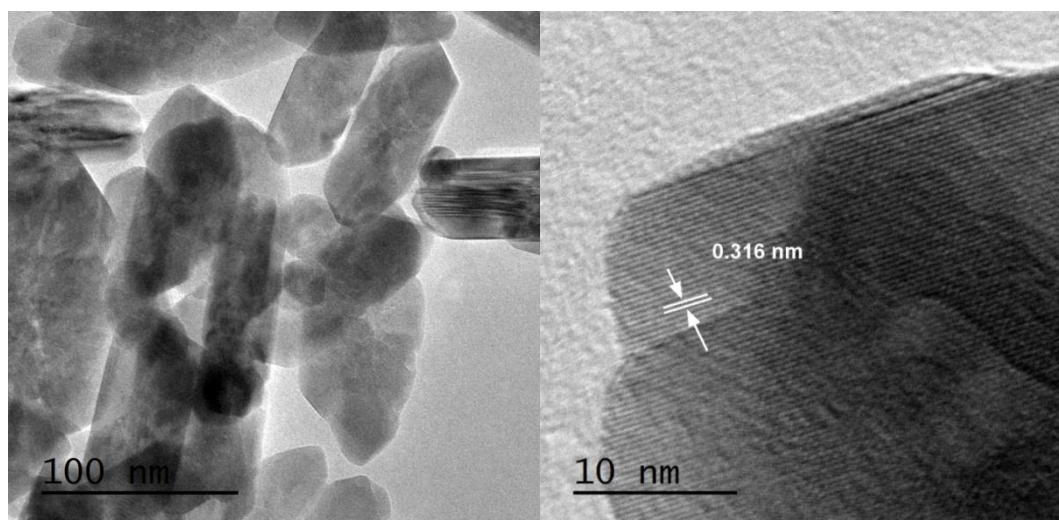| pH	2.6	7.0	11.0	14.0
Particle size (nm)	11.03	12.99	14.76	98.77(L)
				37.57(W)

* L is the length and Wis the width
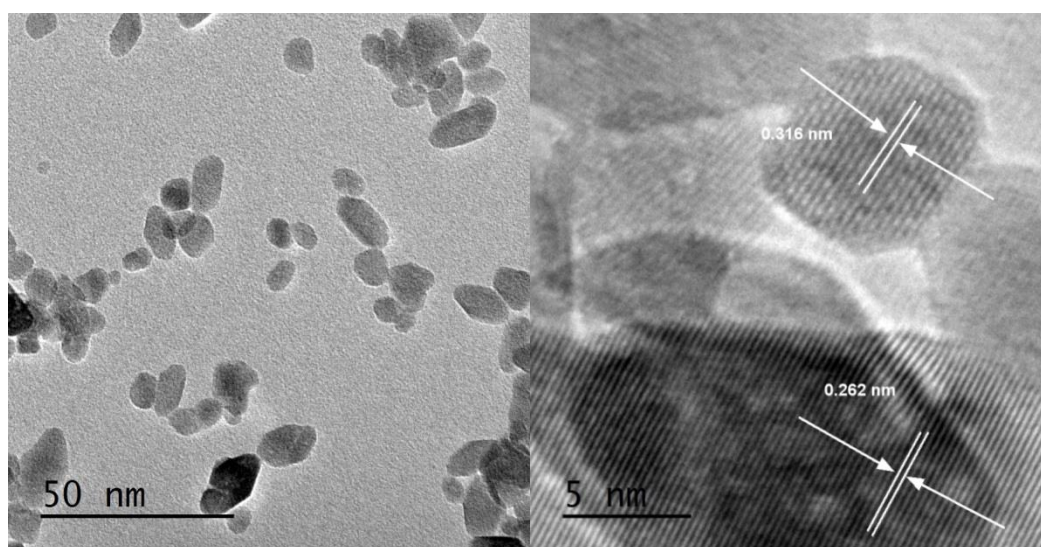
Figure 2. HR-TEM of ZrO_2 sample prepared at pH=2.6.

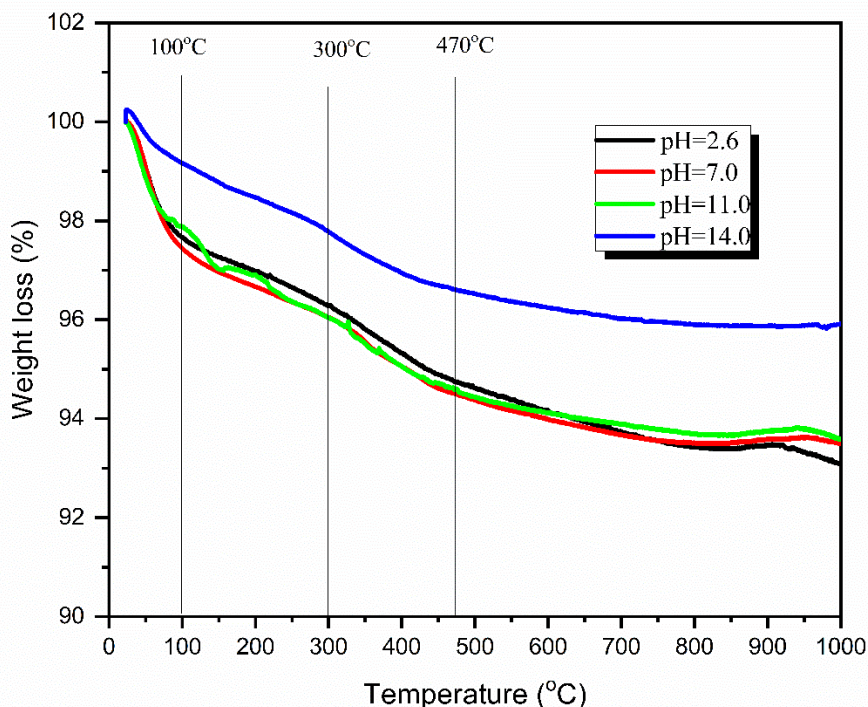**Figure 3.** HR-TEM of ZrO_2 sample prepared at pH=7.0.

Figure 4. HR-TEM of ZrO_2 sample prepared at pH=11.0

Figure 5. HR-TEM of ZrO_2 sample prepared at pH=14.0.

3.3. Thermal analysis

Thermal gravimetric analysis (TGA) of ZrO_2 prepared at different pH are shown in Fig. 6. There are three weight loss regions. The first region between room temperature and 100˚C, the second region between 100-300˚C and the third region between 300-470˚C.
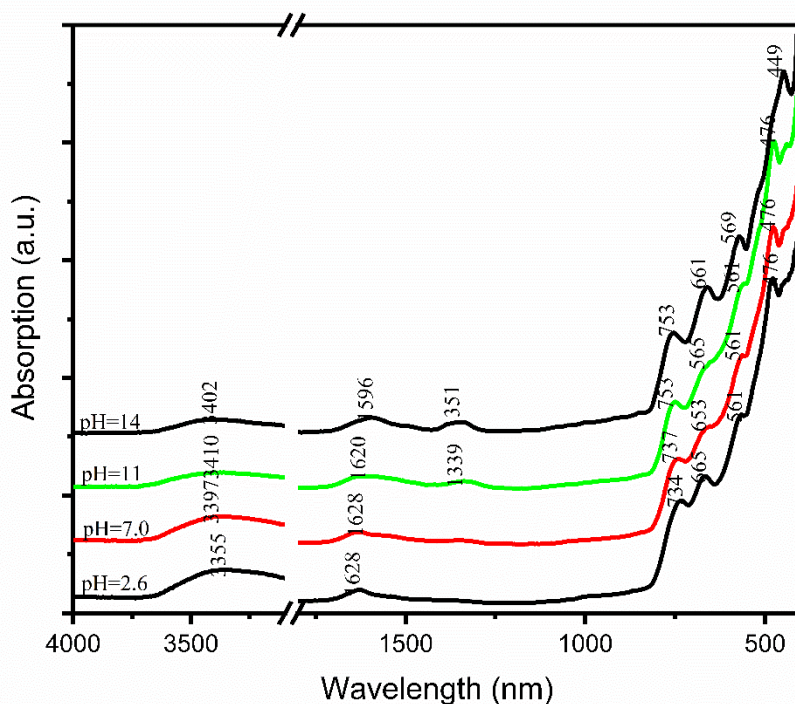

Figure 6. TGA of ZrO_2 sample prepared at different pH.

The weight loss of the first region is due to the desorption of physically adsorbed water [33]. The weight loss in the second region associated with the elimination of chemically bonded of water on the surface. The third region are due to elimination of OH group [34]. The increase in crystallite size leads to a non-monotonic decrease in the amount of physically adsorbed water as well as the total amount of water. Samples prepared at pH from 2.61 to 11 with close particles sizes the total water contents show insignificant changes. However, sample prepared at pH=14 has the highest particle size (89 nm) and the lowest total water content.

3.4. ATR-FTIR Spectroscopy

The ATR-FTIR spectra are used to sense surface functional groups present on ZrO_2 catalysts produced by hydrothermal method. Fig. 7 displays absorption large bands at 3100-3600 cm^{-1} correspond to the stretching of -OH groups. The well-defined bands between 1700-1500 cm^{-1} and 1350 cm^{-1} correspond to the vibration of the hydroxyl groups on ZrO_2 surfaces. The peaks between 450-830 cm^{-1} due to Zr-O bond [33, 35]. In sample of pure monoclinic ZrO_2 (pH=2.61 and pH=14) show stray well-resolved peaks at 560 and 650 cm^{-1} these peaks corresponds to monoclinic phase [36].

**Figure 7.** ATR-FTIR spectra of ZrO_2 sample prepared at different pH.

In biphasic samples (monoclinic and tetragonal phases), the previous two peaks appear less resolved. The number of infrared active mode in monoclinic ZrO_2 is greater than those of tetragonal ZrO_2 due to symmetry of crystal of the monoclinic smaller than tetragonal phase [37]. The band at 1628 cm^{-1} is very broad because water molecules adsorbed with different coordination states. The bands at 1350 and 1330 cm^{-1} are characteristics of the surface O-H groups at different adsorption sites [38]. These bands are more intense in samples with only monoclinic ZrO_2 phase, which produced at both low pH (2.61) and high pH (14). Generally, terminal O-H groups at zirconia surface have two coordination environments; one is coordinated to only one Zr ion and the other is multicoordinated to two or three Zr ions [9, 39].

3.5 Electrocatalysis for hydrogen evolution reaction (HER)

Fig 8 (a) displays the polarization curve of the ZrO_2 catalyst prepared at different pH, with the same electrode mass loading. Measurements were done in 1.0 M NaOH solution, and the potential were scanned at a rate of $5.0\,mV\,s^{-1}$ up to a cathodic potential of -1.5 V. The onset potential (E_{HER}), the potential beyond which the cathodic current is sharply enlarged, to more anodic (active), is important parameter for evaluating the catalytic activity. The onset potentials for all samples are given in Table 3. Catalyst ZrO_2 (pH=2.61) is the best with onset potential -290 mV with more sharp increase in cathodic current beyond E_{HER}. This sharpness means that high cathodic currents (equivalent to huge amount of H_2) can be produced at low potentials. In our previous study we found that repetitive cyclic cathodic

polarization increases the electrocatalytic activity of monoclinic ZrO_2 [10]. On the other hand, other ZrO_2 catalysts required much higher overpotential to obtain the same cathodic current (see Table 3). The present results tell the high HER catalytic performance of ZrO_2 (pH=2.61) catalyst in comparison with other catalysts. The overpotential at 10 mA.cm^{-2} current density (η_{10}) for GC, ZrO_2 (pH=2.61), ZrO_2 (pH=7.0), ZrO_2 (pH=11.0) and ZrO_2 (pH=14.0) are determined as 678, 315, 528, 561 and 479 mV, respectively. An overpotential of 370 mV is needed for ZrO_2 (pH=2.61) to produce current density of 20 mA.cm^{-2}, which is the best performance among all ZrO_2 catalysts.
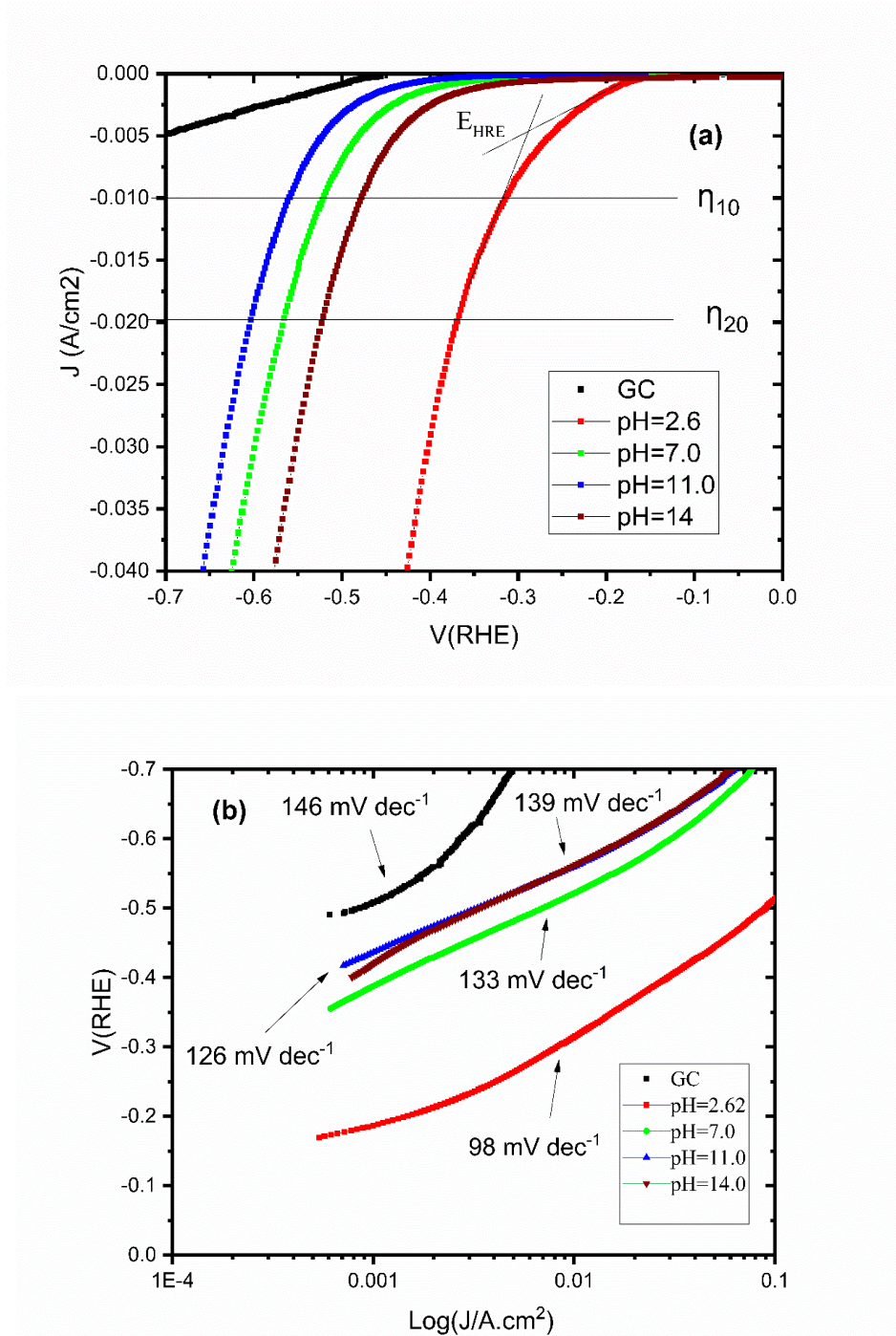
Figure 8. Cathodic polarization measurements **(a)** and the corresponding Tafel plots **(b)** for ZrO_2 catalysts prepared at different pHs.

The electrochemical kinetics parameters used to describe the of the HER reaction were calculated from Fig. 8(b), which created by fitting the linear polarization data of Fig. 8(a) to Tafel equation of. Table 3 also summarizes Tafel slope for each tested catalyst. Tafel slopes are employed to explain the catalytic kinetics of electrocatalysts. A smaller Tafel slope usually indicates faster kinetics. Tafel slopes for catalyst for ZrO_2 (pH=2.61), ZrO_2 (pH=7.0), ZrO_2 (pH=11.0) and ZrO_2 (pH=14.0) were 98, 133, 126, 139 mV.dec^{-1}, respectively (Fig. 8 b).

Table 3. The electrochemical kinetic parameters for the HER on the surfaces of ZrO_2 catalysts prepared at different pHs in NaOH solution (1.0 M).

| Catalyst	E_{HER} mV vs. RHE	Tafel slope $(-\beta_c$, mV dec$^{-1})$	η_{10} (mV vs RHE)	η_{20} (mV vs RHE)
bare GC	------	146	678	----
ZrO_2 (pH=2.62)	-290	98	315	370
ZrO_2 (pH=7.0)	-467	133	528	570
ZrO_2 (pH=11.0)	-505	126	561	604
ZrO_2 (pH=14.0)	-443	139	479	524

* η_{10} is the overpotential at j = 10 mA cm^{-2} (mV vs RHE)

** η_{20} is the overpotential at j = 20 mA cm^{-2} (mV vs RHE)

The HER in alkaline media occurs in steps mechanism. The first step named Vomer step and can represented as following:

$H_2O + S^* + e^- \rightarrow S^*$-$H_{ads} + OH^-$
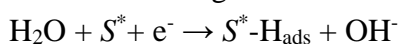
Where S^* represents the active site of the catalyst and S^*-H_{ads} represents the intermediate hydrogen adsorbed on the active site. The second step is either Heyrovsky step or Tafel step, which can be represented as following:

$H_2O + S^*$-$H_{ads} + e^- \rightarrow H_2 + S^* + OH^-$ (Heyrovsky)

S^*-$H_{ads} + S^*$-$H_{ads} \rightarrow S^* + S^* + H_2$ (Tafel)
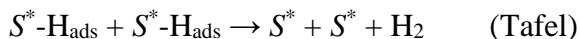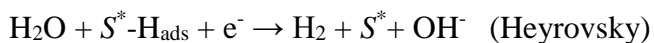
Examining the electrochemical data (Fig. 8) and Tafel slopes (Table 3), we came to conclusion that the active catalytic sites (the -OH functional groups) on monoclinic ZrO_2 enhance hydrogen adsorption in the Volmer mechanistic step.

The slow rate-determining step can be determined from Tafel slope values (Table 3). Conway et.al [40] stated that the rate determining step is Volmer, Heyrovsky, or Tafel step, if the Tafel slope (β_c) is close to the values of 120, 40, or 30 mV.dec^{-1}, respectively. The β_c values of the ZrO_2 catalysts are in between 98 and 139 122 mV dec^{-1}. The after mentioned β_c values are close to the value of Volmer step (120 mV.dec^{-1}), suggesting that Volmer is the rate-determining step in the present catalysts.

4. CONCLUSION

The effect of pH on the phase formation of the ZrO_2 prepared by hydrothermal technique at 240 °C was investigated. The products are monoclinic and tetragonal ZrO_2 phases. At both low and high pHs (2.61 and 14) the products are single phase monoclinic ZrO_2. However, at intermediate pHs (7.0-11.0), the produces are biphasic mixture of monoclinic and tetragonal phase. High-resolution TEM micrographs show that all ZrO_2 samples contain particles in nono size range. The particles size slightly increases (from 11 to 14 nm)) with increasing the pH up to 11. However, at pH=14.0, the particle size abruptly increases to 98 nm. The vibration spectra proved that monoclinic ZrO_2 contain intense surface O-H functional groups, that enhance the electrocatalytic activity of ZrO_2 nanoparticles. The number of peaks present in monoclinic form is higher than those present in tetragonal form due to symmetry of crystal of the monoclinic smaller than tetragonal. The catalytic performance of monoclinic ZrO_2 toward the electrochemical generation of H_2 gas from alkaline solutions significantly exceeded that of the tetragonal ZrO_2 catalysts, especially that produced at low pH=2.61. The high catalytic performance of monoclinic ZrO2 was attributed the abundance of active surface –OH groups. The finding was proved by ATR-FTIR spectroscopy.

References

1. A. Iulianelli, V. Palma, G. Bagnato, C. Ruocco, Y. Huang, N.T. Veziroğlu, A. Basile, *Renewable Energy*, 119 (2018) 834.
2. N. Chen, J. Wang, W. Yin, Z. Li, P. Li, M. Guo, Q. Wang, C. Li, C. Wang, S. Chen, *Royal Society Open Science*, 5 (2018) https://doi.org/10.1098/rsos.171516
3. R. Piticescu, C. Monty, D. Millers, *Sensors and Actuators, B: Chemical*, 109 (2005) 102.
4. J. Grams, M. Niewiadomski, R. Ryczkowski, A.M. Ruppert, W. Kwapiński, *Int. J. Hydrogen Energy*, 41 (2016) 8679.
5. A.V. Shevchenko, E.V. Dudnik, A.K. Ruban, N.V. Danilenko, V.P. Red'ko, *Poroshkovaya Metallurgiya,* (2001) 9.
6. Y. Takahashi, A. Yamada, K. Mizuguchi, T. Kurita, I. Sakaki, F. Sasaki, T. Fujii, T. Tsuji, in: International Conference on Nuclear Engineering, Proceedings, ICONE, 2015.
7. E. Drozdz, *RSC Advances*, 6 (2016) 84752.
8. N. Maragani, K. Vijaya Kumar, *Rasayan Journal of Chemistry*, 10 (2017) 1128.
9. N.Y. Mostafa, Z.I. Zaki, Q. Mohsen, S.H. Alotaibi, A.A. El-moemen, M.A. Amin, *Journal of Molecular Structure*, 1214 (2020).
10. N.Y. Mostafa, M.M. Qhtani, S.H. Alotaibi, Z.I. Zaki, S. Alharthi, M. Cieslik, K. Gornicka, J. Ryl, R. Boukherroub, M.A. Amin, *International Journal of Energy Research*, 44 (2020) 10695.
11. M.K. Loudjani, R. Cortès, *Journal De Physique*. IV : JP, 7 (1997) C2.
12. I. Fatimah, A. Taushiyah, F.B. Najah, U. Azmi, in: IOP Conference Series: *Materials Science and Engineering,* 2018.
13. F. Li, N. Chen, L. Li, Y. Li, Journal of University of Science and Technology Beijing: Mineral Metallurgy Materials (Eng Ed), 7 (2000) 45.
14. C. Gaglieri, R.T. Alarcon, R. de Godoi Machado, D.S.S. Padovini, F.M.L. Pontes, F.J. Caires, *Thermochim. Acta*, 653 (2017) 59.

15. H. Kaneko, T. Okamura, H. Taimatsu, Y. Matsuki, H. Nishida, *Sensors and Actuators B: Chemical*, 108 (2005) 331.
16. A. Savin, M.L. Craus, V. Turchenko, A. Bruma, S. Malo, T.E. Konstantinova, V.V. Burkhovetsky, in: NDT in Progress 2017 - 9th International Workshop NDT in Progress, Proceedings, 2017, pp. 85.
17. M. Monzavi, F. Zhang, T. Douillard, L. Gremillard, S. Noumbissi, H. Nowzari, J. Chevalier, *Journal of the European Ceramic Society*, 40 (2020) 3642.
18. A.V. Shevchenko, E.V. Dudnik, A.K. Ruban, V.P. Red'ko, V.M. Vereschaka, L.M. Lopato, *Powder Metall. Met. Ceram.*, 41 (2002) 558.
19. Y. Han, J. Zhu, *Top. Catal.*, 56 (2013) 1525.
20. X. Hong, S. Xu, X. Wang, D. Wang, S. Li, B.A. Goodman, W. Deng, *Journal of Luminescence*, 231 (2021) 117766.
21. G.P. Cousland, X.Y. Cui, A.E. Smith, A.P.J. Stampfl, C.M. Stampfl, *J. Phys. Chem. Solids*, 122 (2018) 51.
22. N.Y. Mostafa, M.M. Hessien, A.A. Shaltout, *Journal of Alloys and Compounds*, 529 (2012) 29.
23. G.A. El-Shobaky, A.M. Turky, N.Y. Mostafa, S.K. Mohamed, *Journal of Alloys and Compounds*, 493 (2010) 415.
24. Y. Li, P.C. Burns, *J. Nucl. Mater.*, 299 (2001) 219.
25. R. Nacken, Chemiker-Ztg. 74. Jahrg. Nr., 50 (1950) 745.
26. A. Walker, E. Buehler, *Ind. Eng. Chem.*, 42 (1950) 1369.
27. J. Klinowski, *Prog. Nucl. Magn. Reson. Spectrosc.*, 16 (1984) 237.
28. N.Y. Mostafa, M. Hessien, A.A. Shaltout, *J. Alloys Compd.*, 529 (2012) 29.
29. C. Feldmann, C. Metzmacher, *J. Mater. Chem.,* 11 (2001) 2603.
30. C.V. Reddy, B. Babu, I.N. Reddy, *J. Shim, Ceram. Int.*, 44 (2018) 6940.
31. M. Hirano, E. Kato, *J. Ceram. Soc. Jpn.*, 105 (1997) 37.
32. C. Wang, Y. Wang, Y. Cheng, L. Zhu, B. Zou, Y. Zhao, W. Huang, X. Fan, Z.S. Khan, X. Cao, *J. Cryst. Growth*, 335 (2011) 165.
33. D.S.S. Padovini, D.S.L. Pontes, C.J. Dalmaschio, F.M. Pontes, E. Longo, *RSC Advances*, 4 (2014) 38484.
34. M. Picquart, T. López, R. Gómez, E. Torres, A. Moreno, J. Garcia, *J. Therm. Anal. Calorim.*, 76 (2004) 755.
35. A. Singh, U.T. Nakate, *The Scientific World Journal*, 2014 (2014).
36. C. Phillippi, K. Mazdiyasni, *J. Am. Ceram. Soc.*, 54 (1971) 254.
37. H. Ouyang, C. Li, K. Li, H. Li, Y. Zhang, Journal Wuhan University of Technology, *Materials Science Edition*, 31 (2016) 68.
38. G.K. Sidhu, R. Kumar, *Appl. Surf. Sci.*, 392 (2017) 598.
39. S. Kouva, K. Honkala, L. Lefferts, J. Kanervo, *Catalysis Science and Technology*, 5 (2015) 3473.
40. B.E. Conway, B.V. Tilak, *Electrochimica Acta*, 47 (2002) 3571